Online Postfault Strategy of Minimum Copper Loss in Full Torque Operation Range for Dual Three-Phase PMSM Under Single Open-Phase Fault

Kailiang Yu, *Member, IEEE*, Zheng Wang, *Senior Member, IEEE*, Huanzhi Wang, *Graduate Student Member, IEEE*, Chenhao Zhao, *Graduate Student Member, IEEE*, Xuhui Zhu, *Member, IEEE*, and Christopher H. T. Lee, *Senior Member, IEEE*

***Abstract*—Fault-tolerant ability of dual three-phase permanent magnet synchronous motors (PMSMs) is crucial for safety-critical applications. When a single open-phase fault occurs, the current references in conventional methods must be adjusted for avoiding the generation of torque ripple. Meanwhile, their design should balance the tradeoff between the torque operation range (TOR) and the copper loss. However, these postfault current references still need to be retailored under different open-phase fault locations; otherwise, more severe system damage may occur. Aiming to improve the robustness of the control algorithm, this article has proposed an online postfault strategy that can achieve minimum copper loss while maximizing the TOR for dual three-phase PMSMs with sinusoidal back-EMF. Unlike existing literature, the current reference in the harmonic subspace can be uniformly determined by the intermediate variable of phase shift and amplitude ratio, independent of fault scenarios. Additionally, the required fault identification is reduced from locating a specific phase to identifying one set of three-phase windings. The postfault performance of minimum copper loss can be achieved during the full TOR. Furthermore, the implementation of proposed algorithm does not require any optimization iterative process or look-up tables. Comprehensive experimental results have verified the effectiveness of the proposed method.**

***Index Terms*—Dual three-phase permanent magnet synchronous motors (PMSMs), minimum copper loss, online postfault strategy, open-phase fault, torque operation range.**

NOMENCLATURE

a	Derating factor, $a = \|\boldsymbol{I}_{dq}\|/\|\boldsymbol{I}_{rt}\|$.
f	Fault phase such as A, B, C, D, E, F.
$\boldsymbol{F}_{mn}$	Complex vector, $\boldsymbol{F}_{mn} = F_m + jF_n$. The subscript mn can be dq, z1z2, $d1q1$, $d2q2$.
$\boldsymbol{I}$	Current vector. It is typically indexed with subscripts such as 1, 2, and p, n.
$\boldsymbol{I}_{\mathbf{phase}}$	Phasor of phase current.
L_D, L_Q	Direct-axis inductance and quadrature-axis inductance in the torque subspace.
L_{z1}, L_{z2}	Direct-axis inductance and quadrature-axis inductance in the harmonic subspace.
L_d, L_q	Direct-axis and quadrature-axis self-inductance of three-phase windings.
L_σ	Leakage inductance.
M_d, M_q	Direct-axis and quadrature-axis mutual-inductance of three-phase windings.
n_p	Pole pairs of the rotor.
u, i	Voltage and current.
R_s, ψ_m	Stator resistance and rotor flux linkage.
s	Laplace operator.
ω_e, θ_e	Electrical angular speed and position angle.
ω_c	Cut-off frequency of the notch filter.

Superscripts

$*$	Complex conjugate. $(\boldsymbol{F}_{mn})^* = F_m - jF_n$.
ref	Reference value.
T	Matrix transpose.
P, *N*	Positive- and negative-sequence components.

Subscripts

1, 2	Components of the first and second set of three-phase winding.
f	Components under fault operation
$\alpha\beta$ and xy	Components of torque subspace and harmonic subspace in the stationary frame.
dq and z1z2	Components of torque subspace and harmonic subspace in the synchronous rotating frame.
p, n	Positive-sequence and negative-sequence components of three-phase winding.
$d1q1$ and $d2q2$	Components of the first set and the second set of three-phase winding in the synchronous rotating frame.

Received 27 December 2024; revised 4 May 2025; accepted 10 June 2025. Date of publication 17 June 2025; date of current version 5 August 2025. This research was supported in part by A*STAR under its RIE2025 MTC IAF-PP: Development of High Performance Electric Traction Module, Grant No. M22K4a0044, and in part by National Research Foundation (NRF) Singapore under its NRF Fellowship Grant NRF-NRFF12-2020-0003. Recommended for publication by Associate Editor J. He. *(Corresponding author: Christopher H. T. Lee.)*

Kailiang Yu, Huanzhi Wang, Chenhao Zhao, and Christopher H. T. Lee are with the School of Electrical and Electronic Engineering, Nanyang Technological University, Singapore 639798 (e-mail: kailiang.yu@ntu.edu.sg; huanzhi001@e.ntu.edu.sg; chenhao001@e.ntu.edu.sg; chtlee@ntu.edu.sg).

Zheng Wang is with the School of Electrical Engineering, Southeast University, Nanjing 210096, China (e-mail: zwang@eee.hku.hk).

Xuhui Zhu is with the School of Electrical Engineering and Automation, Nantong University, Nantong 226019, China (e-mail: zhuxuhui@ntu.edu.cn).

Color versions of one or more figures in this article are available at https://doi.org/10.1109/TPEL.2025.3580458.

Digital Object Identifier 10.1109/TPEL.2025.3580458

k, θ_{shift}	Amplitude ratio and phase shift of the positive-sequence components between two sets of three-phase windings.
ML, MT	Components of the ML and the MT control strategy.
rt	Rated values of healthy machine.

Matrix[1]

$\boldsymbol{I}_h$, $\boldsymbol{I}_f$	Column vector of six-phase currents under healthy condition and under faulty condition.
$\boldsymbol{I}_{rt}$	Column vector of six-phase rated currents.
$\boldsymbol{T}_{\text{VSD}}$	Transformation matrix of vector space decomposition (VSD).
$\boldsymbol{T}_h$	Postfault current coefficients matrix.

I. Introduction

FAULT-TOLERANT ability of multiphase permanent magnet synchronous motors (PMSMs) drive system, in addition to other features of high power density and lower torque ripple, is receiving more and more attention in safety-critical applications such as aircraft systems, ship propulsion, and wind turbines [1], [2], [3], [4]. As one type of multiphase motors, dual three-phase PMSM drives has recently gained significant attraction owing to the good compatibility for mature three-phase drives. Compared to three-phase PMSM drive system, the dual three-phase PMSM drive system can achieve the control torque-ripple-free performance just by the software reconfiguration under the open-circuit fault [5], [6], which is the most representative among various types such as open-circuit switch faults, high-resistance connections, and current-sensor faults [7].

In order to tackle the coupled relationship between six phase currents, the control scheme of dual three-phase PMSM has widely employed the vector space decomposition (VSD) model [8], [9], where the phase current in the natural stationary reference frame can be mapped into different decoupled two-dimensional (2-D) subspaces such torque subspace and harmonic subspace. During the healthy operation, the currents of torque subspace are determined by the torque generation and air-gap magnetic field adjustment, while the currents in other harmonic subspace can be independently regulated and are typically set to zero for the lowest copper loss [9]. After the occurrence of open-circuit fault, the current references in these harmonic subspaces need to be modified from zero to some specific value for regulating the remained healthy phase current, thereby maintaining the same rotating airgap magnetomotive force [10]. That is to say, the currents between different subspaces are no longer independent for dual three-phase PMSM under the faulty condition. In order to guarantee the torque-ripple-free performance, the current references in harmonic subspace need to be rewritten as the linear combination of the currents in torque space, where these current coefficients must comply the constraint imposed by the single-phase open-circuit fault [11].

After the single open-phase fault, in addition to the two control degrees of freedom used for the torque-ripple-free performance, the remaining one can be utilized for choosing the current coefficients, which has an impact on the system postfault performance. In term of the copper loss and the achievable torque range, there are mainly three types of postfault control strategies, namely, minimum losses (ML) [12], maximum torque (MT) [13], and full-range minimum losses (FRML) [14]. In ML strategy, these current coefficients are optimized for the lowest copper loss under a given torque [12]. However, it would result in the unbalanced amplitude of phase current, which further brings another challenge of the power derating under the amplitude limit of phase current. For expanding the torque operation range (TOR), the maximum amplitude of phase currents is minimized in the MT strategy [13], which causes the greater copper loss than that of ML strategy. In order to achieve the lowest copper loss and the entire TOR simultaneously, the FRML strategy has been investigated for the optimization of these current coefficients [14]. Yet, these coefficients in [14], which vary with the variation of torque current, are complex to online solve and are, therefore, numerically calculated by the offline FRML. Hence, many look-up tables are used for coefficient prestorage in the digital controller, which, in turn, increases the usage of computational resources. In addition, as reported in [15], [16], [17], and [18], injecting current harmonics into the harmonic subspace (nontorque-producing subspace) can further extend the torque range while keeping phase current within its limits. However, this approach leads to nonsinusoidal postfault current references, which is beyond the scope of this study.

To reduce the computational burden, the online calculation strategies [19], [20], [21], [22] has been proposed for pursuing the same performance as FRML strategy. As reported in [20], the novel online iteration process has been employed from the extrapolation from single-phase faults to multiphase faults. Meanwhile, many researchers have founded that the FRML can be interpreted as a mixture between the ML strategy and the MT strategy [21], [22]. These online postfault control strategies determine the optimal mixing ratio of current coefficients—derived from the ML and MT strategies—either approximately, using linear closed-form expressions [21], or more accurately, by evaluating the maximum current amplitude [22]. It should be pointed out that those above postfault optimization strategies are designed within the control framework of active fault-tolerant control method, where fault diagnosis and location are necessary for the implementation. In addition, these current coefficients of postfault control strategies need to be tailored under different open-phase fault scenarios. What is worse, the misleading result of fault diagnosis would lead to the torque ripples, even the breakdown of drive system.

Aiming to reduce dependency on fault-diagnosis, the control schemes with natural fault-tolerant performance (also referred to passive or diagnosis-free self-healing) [23], [24], [25], [26] have been investigated as a promising alternative. Although torque-ripple-free performance can be achieved without the need for fault diagnosis, they also introduce another challenge: the inability to regulate postfault performance [7] due to the absence

[1]It should be noted that other boldface italic symbols represent complex vectors unless otherwise specified.

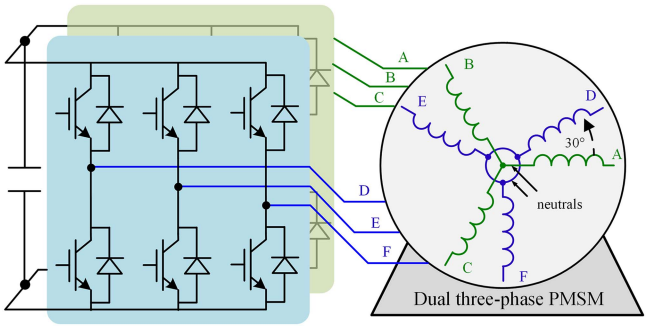

Fig. 1. Stator winding configuration of dual three-phase PMSM drives.

of optimization variables or an uncontrolled self-adaptation process.

As reported in another universal control scheme [27], the negative-sequence components of harmonic subspace are eliminated by the notch filter in the universal control scheme while the positive-sequence ones are employed for realizing the adjustment of postfault performance. By introducing new optimization variables—amplitude ratio and phase shift—the ML strategy was first developed in [27] for natural fault-tolerant control. Subsequently, the settings for amplitude ratio and phase shift were derived in [28] for the MT strategy. Additionally, an approximate FRML strategy can be achieved through the linear combination of the two aforementioned settings [29]. To the best knowledge of the authors, there are little studies about the combination between the universal control scheme and the FRML strategy.

Although several online postfault control strategies have been developed to approximate the behavior of offline FRML method, some differences in copper loss performance still remain. Furthermore, these postfault current references still need to be retailored under different open-phase fault locations. Aiming to fill this gap, this article develops an online postfault strategy of minimum copper loss in full TOR for dual three-phase PMSM with isolated neutral points under single open-phase fault. It should be noted that the effects of space harmonics in the back-EMF are not considered in this study, as they can be effectively minimized through appropriate stator winding design. The rest of this article is organized as follows. First, the model and existing postfault strategies of dual three-phase PMSM have been briefly introduced in Section II. Then, the detailed settings of the amplitude ratio and the phase shift have been derived for proposed online postfault control strategy in Section III. At last, the experiments verification presents in Sections IV. Finally, Section V concludes this article.

II. Background

A. Modeling of Dual Three-Phase PMSM

As shown in Fig. 1, the stator winding of dual three-phase PMSM can be split into two sets of three-phase windings, one of which is denoted as Phase A, Phase B, and Phase C, while the second set is represented by Phase D, Phase E, and Phase F, respectively. In this article, the neutral points of two sets of three-phase windings are isolated from each other for avoiding the zero-sequence current, thereby simplifying the control method of the motor system.

Aiming to solve the coupled relationship between phase variables, the phase variables in the natural stationary reference frame can be mapped into a series of 2-D orthogonal subspaces by the transformation matrix $\boldsymbol{T}_{\mathrm{VSD}}$ [8], as given by

$$\begin{bmatrix} l_\alpha \\ l_\beta \\ l_x \\ l_y \\ l_{o1} \\ l_{o2} \end{bmatrix} = \underbrace{\frac{1}{6}\begin{bmatrix} 2 & -1 & -1 & \sqrt{3} & -\sqrt{3} & 0 \\ 0 & \sqrt{3} & -\sqrt{3} & 1 & 1 & -2 \\ 2 & -1 & -1 & -\sqrt{3} & \sqrt{3} & 0 \\ 0 & -\sqrt{3} & \sqrt{3} & 1 & 1 & -2 \\ 2 & 2 & 2 & 0 & 0 & 0 \\ 0 & 0 & 0 & 2 & 2 & 2 \end{bmatrix}}_{\boldsymbol{T}_{VSD}} \begin{bmatrix} l_{\mathrm{A}} \\ l_{\mathrm{B}} \\ l_{\mathrm{C}} \\ l_{\mathrm{D}} \\ l_{\mathrm{E}} \\ l_{\mathrm{F}} \end{bmatrix} \tag{1}$$

where the symbol l denotes machine variables. It can be observed that, due to the isolated neutral points, the sum of the three-phase currents in each set of three-phase windings is zero according to Kirchhoff's current law. Consequently, the zero-sequence subspace currents are inherently zero through the VSD transformation and will not be considered in the subsequent analysis.

Like three-phase motor drive, the components of torque subspace and harmonic subspaces can be further transformed into synchronous rotating reference frame [27], as given by

$$\begin{cases} \boldsymbol{F}_{dq} = \boldsymbol{F}_{\alpha\beta} e^{-j\theta_e} \\ \boldsymbol{F}_{z1z2} = \boldsymbol{F}_{xy} e^{j\theta_e} \end{cases}. \tag{2}$$

Assuming that the space harmonics of the back-EMF are negligible, the dynamic model of dual three-phase PMSM in the synchronous rotating coordinate frame can be obtained by VSD as follows [27]:

$$\begin{cases} u_d = R_s i_d + L_D \frac{di_d}{dt} - \omega_e L_Q i_q \\ u_q = R_s i_q + L_Q \frac{di_q}{dt} + \omega_e (L_D i_d + \psi_m) \\ u_{z1} = R_s i_{z1} + L_{z1} \frac{di_{z1}}{dt} + \omega_e L_{z2} i_{z2} \\ u_{z2} = R_s i_{z2} + L_{z2} \frac{di_{z2}}{dt} - \omega_e L_{z1} i_{z1} \end{cases}. \tag{3}$$

It should be pointed out that the mutual inductance is incorporated into the inductance of the harmonic subspace and the torque subspace in the VSD model [9] as illustrated by

$$\begin{aligned} L_D &= L_d + M_d, L_Q = L_q + M_q \\ L_{z1} &= L_d - M_d, L_{z2} = L_q - M_q \end{aligned} \tag{4}$$

where the self-inductance and mutual inductance of three-phase stator windings can be further separated into leakage and mutual components, expressed as $L_d = L_\sigma + M_d$, $L_q = L_\sigma + M_q$. Therefore, the inductance of harmonic subspace can be simplified as $L_{z1} = L_{z2} = L_\sigma$ in most cases.

On the other hand, the current vectors of different subspaces in VSD model can be also calculated by two sets of three-phase units in double dq model in [27] as

$$\begin{cases} \boldsymbol{F}_{dq} = 0.5(\boldsymbol{F}_{d1q1} + \boldsymbol{F}_{d2q2}) \\ \boldsymbol{F}_{z1z2} = 0.5(\boldsymbol{F}_{d1q1} - \boldsymbol{F}_{d2q2})^* \end{cases}. \tag{5}$$

It can be inferred from the position of rotor flux linkage in (3) that the electromechanical energy conversion is determined by the components of torque subspace due to the interaction

between the back-electromotive force and the currents of torque subspace. More specifically, the torque of dual three-phase PMSM can be calculated as

$$T_e = 3n_p[\psi_m + (L_D - L_Q)i_d]i_q. \tag{6}$$

Hence, the current components of harmonic subspace should be controlled to zero for reducing the copper loss.

B. Current References Under Fault-Tolerant Operation

Under a healthy condition, the phase currents of the dual three-phase machine can be expressed as $\boldsymbol{I}_h = [i_{\rm A}\ i_{\rm B}\ i_{\rm C}\ i_{\rm D}\ i_{\rm E}\ i_{\rm F}]^T$. From the perspective view of the VSD model, the currents can be mapped into different subspaces as given by

$$\begin{aligned}\boldsymbol{T}_{\rm VSD}\boldsymbol{I}_h &= \begin{bmatrix} i_\alpha & i_\beta & i_x & i_y & i_{o1} & i_{o2}\end{bmatrix}^T \\ &= \underbrace{\begin{bmatrix} I\cos\theta & I\sin\theta\end{bmatrix}}_{\rm Torquesubspace} \quad \underbrace{0\quad 0}_{\rm Harmonicsubspace} \quad \underbrace{0\quad 0}_{\rm Zero-sequence}^T\end{aligned} \tag{7}$$

where I and θ are the amplitude and phase angle of the current vector ($i_{\alpha\beta} = i_\alpha + ji_\beta$) in torque subspace, respectively. The currents in harmonic subspace i_{xy} are set to zero for reducing the copper loss. The currents in $o1o2$ subspace are always zero owing to the motor configuration of isolated neutral points.

Without the loss of the generality, it is assumed that open-circuit fault occurs in phase A. As reported in [11], the torque equation of (6) is suitable for both the healthy condition and the faulty condition. That is to say, the torque-ripple-free performance can be achieved if the currents of torque subspace remain unchanged during postfault condition as

$$\begin{aligned}\boldsymbol{T}_{\rm VSD}\boldsymbol{I}_f &= \boldsymbol{T}_{\rm VSD}\begin{bmatrix}0 & i_{{\rm B}f} & i_{{\rm C}f} & i_{{\rm D}f} & i_{{\rm E}f} & i_{{\rm F}f}\end{bmatrix}^T \\ &= \begin{bmatrix} I\cos\theta & I\sin\theta & i_{xf} & i_{yf} & 0 & 0\end{bmatrix}^T.\end{aligned} \tag{8}$$

Taking the orthogonal current of torque subspace like i_α, i_β as the basis, the harmonic subspace current of conventional active fault-tolerant control method can be expressed as their linear combination [11] under any postfault condition

$$\begin{bmatrix} i_{xf} \\ i_{yf}\end{bmatrix} = \underbrace{\begin{bmatrix} h_1 & h_2 \\ h_3 & h_4\end{bmatrix}}_{\boldsymbol{T}_h}\begin{bmatrix} i_\alpha \\ i_\beta\end{bmatrix}. \tag{9}$$

It should be noted that these four coefficients, such as h_1, h_2, h_3, and h_4 in the matrix of$\boldsymbol{T}_h$, must also satisfy the current constraints imposed by the fault phase. In other words, these coefficients must be constrained within the feasible region. Furthermore, the feasible region for these coefficients varies depending on the fault location, as detailed in the Appendix.

C. Postfault Strategy of Universal Control Scheme

Different from the active fault-tolerant control method, the universal control scheme shown in Fig. 2 has been developed for the perspective of the frequency domain. Notch filters are employed in the control loop of harmonic subspace of the universal control scheme to separate the negative-sequence components of the harmonic subspace, while retaining the positive-sequence components for postfault performance adjustment. In order to

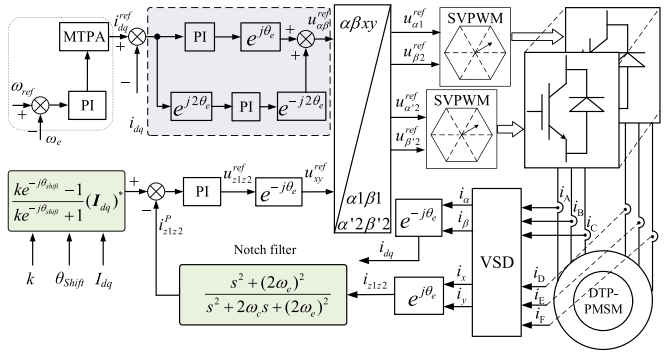

Fig. 2. Universal control scheme for dual three-phase PMSM drive with single phase open-circuit fault [27].

enhance robustness against parameter variations, proportional-integral controllers have been employed to ensure strong tracking performance in the control loop of the harmonic subspace. More details of the frequency components are introduced in the following section.

It can be summarized that the negative-sequence current components of the harmonic subspace represent the constraints introduced by a single-phase open-circuit fault. Therefore, by employing a notch filter to eliminate these components, the universal control scheme can achieve torque-ripple-free performance without the need of fault diagnosis. The transfer function of a notch filter can be expressed as

$$H(s) = \frac{s^2 + (2\omega_e)^2}{s^2 + 2\omega_c s + (2\omega_e)^2}. \tag{10}$$

ω_c is the cut-off frequency associated with the bandwidth of attenuation. As reported in [24], the range of cut-off frequency is usually 2–5 rad/s, which can achieve a good balance between the suppression capability and dynamic performance. The notch frequency is specifically designed to be twice of the fundamental frequency ($2\omega_e$) in order to eliminate the negative-sequence components.

Therefore, the current reference of harmonic subspace determined by the intermediate variable of phase shift and amplitude ratio can be expressed under any fault locations [27]

$$\boldsymbol{I}_{z1z2\_ref} = \frac{ke^{-j\theta_{\rm shift}} - 1}{ke^{-j\theta_{\rm shift}} + 1}(\boldsymbol{I}_{dq})^* \tag{11}$$

where the amplitude ratio (k) and the phase shift ($\theta_{\rm shift}$) of the positive-sequence components in two sets of three-phase windings are defined as

$$k = \|\boldsymbol{I}_{p1}\| / \|\boldsymbol{I}_{p2}\|, \theta_{\rm shift} = \theta_{p1} - \theta_{p2}. \tag{12}$$

It can be inferred from the variable definitions that the amplitude ratio k ranges from 0 to ∞, while the phase shift $\theta_{\rm shift}$ spans from 0 to 2π. Compared to these coefficients of $\boldsymbol{T}_h$, the feasible regions of optimization variable like k and $\theta_{\rm shift}$ are not restricted by fault location. These advantages of optimization variable in universal control scheme makes it more suitable for implementing the postfault optimization control strategy.

At first, the ML strategy of the universal control scheme has been investigated for the dual three-phase PMSM in [27]. And the set of the amplitude ratio and the phase shift (k, θ_{shift}) in the ML strategy can be rewritten as

$$(k,\theta_{\text{shift}})|_{\text{ML}}=\begin{cases}(1/3,0) & f\in\{\text{A},\text{B},\text{C}\}\\ (3,0) & f\in\{\text{D},\text{E},\text{F}\}\end{cases}. \tag{13}$$

The maximum amplitude of torque current of ML strategy is referred to as $\|\boldsymbol{I}_{\alpha\beta}\|_{\text{ML}}$, with a normalized value of $2/\sqrt{13}$.

In addition, in order to extend the operation torque range, the set of the amplitude ratio and the phase shift (k, θ_{shift}) in the MT strategy [28] can be rewritten as

$$(k,\theta_{\text{shift}})|_{\text{MT}}=(1,0). \tag{14}$$

The maximum amplitude of torque current of MT strategy is referred to as $\|\boldsymbol{I}_{\alpha\beta}\|_{\text{MT}}$, with a normalized value of $1/\sqrt{3}$.

In the semi-FRML strategy [29], the linear interpolation of current amplitude ratio k between the ML strategy and the MT strategy is developed as

$$k=k_{\text{ML}}+\frac{k_{\text{MT}}-k_{\text{ML}}}{\|I_{\alpha\beta}\|_{\text{MT}}-\|I_{\alpha\beta}\|_{\text{ML}}}(I_{\text{torque}}-\|I_{\alpha\beta}\|_{\text{ML}}),\theta_{\text{shift}}=0 \tag{15}$$

where I_{torque} is related to the actual amplitude of torque current

$$I_{\text{torque}}=\begin{cases}\|I_{\alpha\beta}\|_{\text{ML}} & \|I_{\alpha\beta}\|\le\|I_{\alpha\beta}\|_{\text{ML}}\\ \|I_{\alpha\beta}\| & \|I_{\alpha\beta}\|\ge\|I_{\alpha\beta}\|_{\text{ML}}\end{cases}. \tag{16}$$

However, the approximate interpolation can only ensure the same performance as the FRML strategy within the torque range below $\|\boldsymbol{I}_{\alpha\beta}\|_{\text{ML}}$ and at the torque point of $\|\boldsymbol{I}_{\alpha\beta}\|_{\text{MT}}$. The copper loss during the torque transition range between $\|\boldsymbol{I}_{\alpha\beta}\|_{\text{ML}}$ and $\|\boldsymbol{I}_{\alpha\beta}\|_{\text{MT}}$ remains higher than that of the FRML strategy. To fill this gap, this article studies the fully equivalent FRML strategy within the control frame of universal control scheme.

III. Proposed Online Postfault Control Strategy

A. Frequency Analysis of Fault-Tolerant Current

As reported in [14], the objective function of FRML control strategy is to minimize the copper losses under a given current of torque subspace, which can be normalized with respect to the rated copper losses in healthy situation as follows:

$$G=\frac{R_s(\boldsymbol{I}_f)^T\boldsymbol{I}_f}{R_s(\boldsymbol{I}_{rt})^T\boldsymbol{I}_{rt}}=\frac{\sum R_s(i_{mf})^2,m=\text{A},\text{B},\ldots,\text{F}}{\sum R_s(i_{m\_rt})^2,m=\text{A},\text{B},\ldots,\text{F}} \tag{17}$$

subject to the restrictions

$$\text{C1}: i_f=\boldsymbol{I}_f[g]=0 \tag{18}$$

$$\text{C2}: \boldsymbol{I}_f[n]\le I_{rt},n=1,2,\cdots,6 \tag{19}$$

where the index g is the corresponding row of the faulty phase in the matrix.

It should be noted that the above objective function is established in the time domain. However, since different sequence components in the frequency domain are analyzed in the development of the proposed control method, a frequency analysis of the fault-tolerant current will be presented.

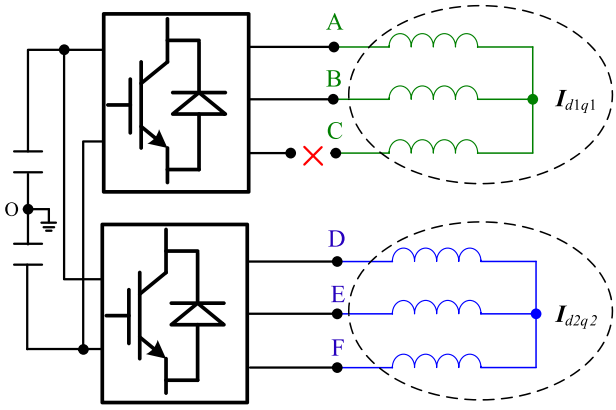

Fig. 3. System connection of dual three-phase PMSM drives with an open-circuit fault in the first set of three-phase winding.

Without the loss of generality, the open-circuit fault is assumed to occurs in the first set of three-phase windings (ABC) as shown in Fig. 3. Due to the presence of the open-circuit fault, negative-sequence components, in addition to the positive-sequence components, are introduced into the current vector of the first set of three-phase windings. These components can be calculated from the imbalanced three-phase currents using the stationary and rotating frame transformations, as given by

$$\boldsymbol{I}_{d1q1}=\underbrace{I_{p1}e^{j\theta_{p1}}}_{\text{positive-sequence}}+\underbrace{I_{n1}e^{j(-2\theta_e-\theta_{n1})}}_{\text{negative-sequence}}. \tag{20}$$

Given that the current in the torque subspace can be considered as the sum of the currents from the two sets of three-phase windings according to (5), the additional ac components will be introduced into the torque subspace by the faulty set. To mitigate this issue, the healthy set should generate components that offset those introduced by the faulty set in (20), as illustrated by

$$\boldsymbol{I}_{d2q2}=I_{p2}e^{j\theta_{p2}}-I_{n1}e^{j(-2\theta_e-\theta_{n1})}. \tag{21}$$

Substituting (20) and (21) into (5), the current vector of different subspaces in the dual three-phase PMSM under fault-tolerant operation can be rewritten as

$$\boldsymbol{I}_{dq}=0.5(I_{p1}e^{j\theta_{p1}}+I_{p2}e^{j\theta_{p2}}) \tag{22}$$

$$\boldsymbol{I}_{z1z2}=\underbrace{0.5(I_{p1}e^{j\theta_{p1}}-I_{p2}e^{j\theta_{p2}})^*}_{\boldsymbol{I}^P_{z1z2}}+\underbrace{I_{n1}e^{j(2\theta_e+\theta_{n1})}}_{\boldsymbol{I}^N_{z1z2}}. \tag{23}$$

Substituting (12) into (22) and (23), the positive-sequence currents of different subspaces can be updated as

$$\begin{cases}\boldsymbol{I}_{dq}=0.5(ke^{j\theta_{\text{shift}}}+1)I_{p2}e^{j\theta_{p2}}\\ \boldsymbol{I}^P_{z1z2}=0.5(ke^{j\theta_{\text{shift}}}-1)^*I_{p2}e^{-j\theta_{p2}}\end{cases}. \tag{24}$$

It can be observed that the positive-sequence components between the torque subspace and the harmonic subspace can be related through the earlier equation in (11).

B. Proposed Online FRML Method

According to Paswal's theorem, the total copper loss calculated in time domain can be transformed into the quadratic sum

of magnitudes of different sequence components in frequency domain as

$$P_{cu} = \frac{R_s}{T}\int_t^{t+T}\sum (i_{mf})^2 = 3R_s\left(\|\boldsymbol{I}_{dq}\|^2 + \left\|\boldsymbol{I}^P_{z1z2}\right\|^2 + \left\|\boldsymbol{I}^N_{z1z2}\right\|^2\right) \tag{25}$$

where T is the period of the fundamental current.

Substituting (24) and (23) into (25), the copper loss of stator windings can be rewritten as

$$P_{cu} = \frac{6k^2+2}{k^2+2k\cos\theta_{\text{shift}}+1}\cdot 3R_s\|\boldsymbol{I}_{dq}\|^2. \tag{26}$$

By employing the new optimization variables, the objective function of FRML control strategy in (17) of Section III-A can be updated as

$$\min G = a^2\cdot \min_{\substack{k\in(0,\infty)\\ \theta_{\text{shift}}\in[0,2\pi)}} \frac{6k^2+2}{k^2+2k\cos\theta_{\text{shift}}+1} \tag{27}$$

subject to the restriction

$$\text{C2}: \boldsymbol{I}_f[n] \le \|\boldsymbol{I}_{rt}\|, n = 1,2,\cdots,6 \tag{28}$$

where the derating factor a stands for the normalized torque current with respect to the rate phase current as illustrated by $a = \|\boldsymbol{I}_{dq}\|/\|\boldsymbol{I}_{rt}\|$. According to the conclusion in [13], the range of a is from 0 to $1/\sqrt{3}$.

It can be inferred from (22) and (23) that the negative-sequence components of the harmonic subspace represent the constraints introduced by the single-phase open-circuit fault. Since these components are separated by a notch filter, the remaining positive-sequence components determined by θ_{shift} and k would not be affected by the single open-phase fault. Therefore, the constraint C1 in (18) imposed by the single open-phase fault does not need to be considered thanks to the adaptation of new optimization variables of k and θ_{shift}.

Remark 1: The minimum value of objective function in (27) representing copper loss can be achieved if and only if the phase shift is zero ($\theta_{\text{shift}} = 0$) under any fixed value of k.

Compared to the traditional mathematical representation from (17) to (19), the feasible regions of new optimization variable can get rid of the restriction from the equality constraints like C1 in (18), thereby being only determined by the inequality constraints of phase current amplitude in (28). As far as the objective function is concerned, the optimization results of multivariate function are easy to be acquired.

In addition, the amplitude of each phase current can be derived from the different sequence components of the three-phase windings, as shown in (20) and (21). Fortunately, this current amplitude model under fault-tolerant conditions has already been investigated in previous research [28]. Based on the conclusions presented in [28], the maximum amplitude of the phase current, normalized with respect to the torque current, can be

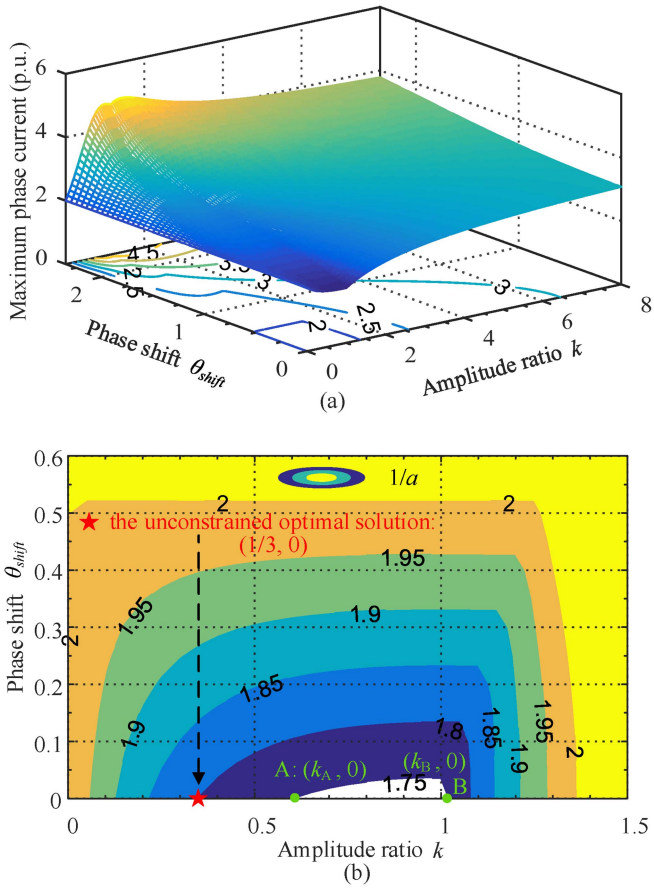

Fig. 4. Constraints of optimization variable in C2 for the proposed fault-tolerant control strategy under the variation of torque current. (a) Normalized maximum phase current M. (b) Feasible region of amplitude ratio k and phase shift θ_{shift} in C2 under different torque currents.

expressed as

$$M = \max_{n=1,2,\cdots,6}\frac{\boldsymbol{I}_f[n]}{\|\boldsymbol{I}_{dq}\|} = \max_{\substack{k\in(0,\infty)\\ \theta_{\text{shift}}\in[0,2\pi)}}\left\{\frac{2\sqrt{3}k, g_{\text{A}}, g_{\text{B}}, g_{\text{C}}}{\sqrt{k^2+1+2k\cos\theta_{\text{shift}}}}\right\} \tag{29}$$

where g_{A}, g_{B}, and g_{C} are the current amplitudes of healthy three-phase windings, and they can be further expressed as

$$\begin{cases} g_{\text{A}}(k,\theta_{\text{shift}}) = 2\sqrt{k^2+1-2k\cos\theta_{\text{shift}}} \\ g_{\text{B}}(k,\theta_{\text{shift}}) = 2\sqrt{k^2+1-2k\cos(\theta_{\text{shift}}+2\pi/3)} \\ g_{\text{C}}(k,\theta_{\text{shift}}) = 2\sqrt{k^2+1-2k\cos(\theta_{\text{shift}}-2\pi/3)} \end{cases}. \tag{30}$$

After obtaining the maximum amplitude of phase current M, the restriction in C2 can be updated by substituting (29) into (28), as given by

$$\text{C2}: M = \max_{\substack{k\in(0,\infty)\\ \theta_{\text{shift}}\in[0,2\pi)}}\left\{\frac{2\sqrt{3}k, g_{\text{A}}, g_{\text{B}}, g_{\text{C}}}{\sqrt{k^2+1+2k\cos\theta_{\text{shift}}}}\right\} \le \frac{\|\boldsymbol{I}_{rt}\|}{\|\boldsymbol{I}_{dq}\|} = \frac{1}{a}. \tag{31}$$

Fig. 4 illustrates the constraint imposed by (31) under varying torque current amplitudes. Specifically, Fig. 4(a) presents the left-hand side of the inequality—i.e., the maximum phase current amplitude M—as a function of the optimization variables θ_{shift} and k. When the right-hand-side term of the inequality

is introduced, the feasible region of optimization variable θ_{shift} and k is visualized in Fig. 4(b), showing how it changes with different torque current amplitudes.

1) By ignoring the inequality constraints in (27), the unconstrained optimal solution of the objective function can be achieved when $k = 1/3$ and $\theta_{\text{shift}} = 0$, as given by

$$\min_{k=1/3,\theta_{\text{shift}}=0} G = 1.5\|\boldsymbol{I}_{dq}\|^2/\|\boldsymbol{I}_{rt}\|^2 = 1.5a^2. \quad (32)$$

2) When the inequality constraints C2 of (31) into consideration, the feasible region of optimization variable may change with the variation of given torque currents. Therefore, a classification discussion will be conducted based on the inclusion relationship between the feasible region and the unconstrained optimal solution ($k = 1/3$, $\theta_{\text{shift}} = 0$) as follows.

I. *Included in Feasible Region*: As shown in Fig. 4(b), the optimal solution is included in feasible region if the torque current is low. Hence, the solution of FRML control strategy can be achieved when $k = 1/3$ and $\theta_{\text{shift}} = 0$. Meanwhile, substituting the optimal solution into (29), the maximum value of phase current at the optimal solution should be not greater than the rated value

$$\max_{k=1/3,\theta_{\text{shift}}=0} \left\{ \frac{2\sqrt{3}k, g_{\text{A}}, g_{\text{B}}, g_{\text{C}}}{\sqrt{k^2+1+2k\cos\theta_{\text{shift}}}} \right\} = \frac{\sqrt{13}}{2} \le \frac{1}{a}. \quad (33)$$

Hence, the normalized torque current of a under condition I is from 0 to $2/\sqrt{13}(\approx 0.55)$.

II. *Excluded in Feasible Region:* When the amplitude of torque current is higher than 0.55, the unconstrained optimal solution would be excluded in feasible region. The feasible region Ω becomes one continuous area, surrounded by the line AB in the x-axis and other boundaries. According to the Remark 1, the optimal point will be located the x-axis line ($\theta_{\text{shift}} = 0$) and other boundaries. It is interesting from Fig. 4 that the feasible region is always be concave area from the view of the line AB, which also means the value of amplitude ratio k in other boundaries is still in the range of the line AB in the x-axis. Therefore, the optimal point of the feasible region must be located in the line AB in the x-axis ($\theta_{\text{shift}} = 0$), which can be expressed by

$$\min_{\Omega} G = \min_{\substack{\Omega:\theta_{\text{shift}}=0 \\ k\in\text{LineAB}}} G = a^2 \cdot \min_{k\in\text{LineAB}} \frac{6k^2+2}{k^2+2k+1}. \quad (34)$$

As shown in Fig. 4, the point A and point B is the projection of the contour lines on the x-axis (the phase shift is zero $\theta_{\text{shift}} = 0$). And their detailed value of k can be calculated as

$$\max\left\{ \frac{2\sqrt{3}k}{\sqrt{k^2+1+2k}}, \frac{2\sqrt{k^2+1+k}}{\sqrt{k^2+1+2k}} \right\} = \frac{1}{a}. \quad (35)$$

Then, the solution of the equation can be derived from

$$k_{\text{A}} = \eta(b) = \frac{b-2-\sqrt{4b-12}}{4-b}, k_{\text{B}} = \frac{b+2\sqrt{3b}}{12-b} \quad (36)$$

where k_{A} and k_{B} are the x-axis values of the point A and the point B, respectively. The variable b can be expressed by $b = 1/a^2$. The relative magnitude relationship between the two variables is $k_{\text{A}} \le 1 \le k_{\text{B}}$.

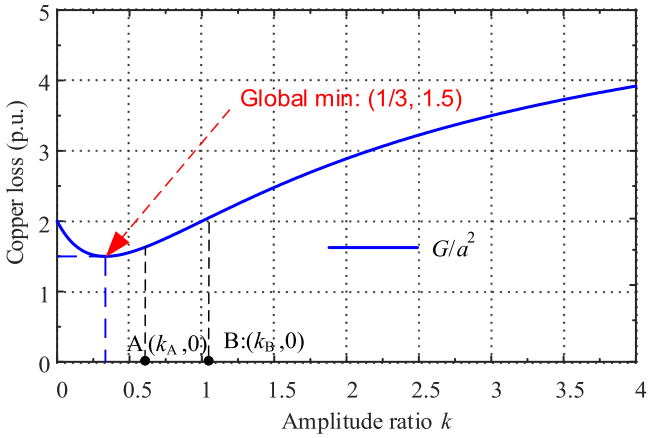

Fig. 5. Copper loss of stator windings G/a^2 with respect to the amplitude ratio k (the phase shift is zero) under the fault-tolerant operation.

In addition, the copper loss of stator windings in (27) under $\theta_{\text{shift}} = 0$ can be illustrated in Fig. 5. When the phase shift k is within the range from 0 to 1/3, the copper loss decreases with the increase of k. On the other hand, the copper loss increases with the increase of k when k is greater than 1/3. Therefore, the optimal point is located on the point A.

Then, the solution of the objective function in (34) the feasible region Ω can be expressed as

$$\min_{\Omega} G = \min_{\substack{\theta_{shift}=0 \\ k\in(k_{\text{A}},k_{\text{B}})}} G = \min_{\substack{\theta_{shift}=0 \\ k=k_{\text{A}}}} G = a^2 \frac{6k_{\text{A}}^2+2}{k_{\text{A}}^2+2k_{\text{A}}+1} \quad (37)$$

where the maximum value of k_{A} in (36) can be achieved when the value of b ($b = 1/a^2$) is 3 under the MT strategy, as expressed by

$$k_{\text{A,max}} = \eta(b=3) = \left.\frac{b-2-\sqrt{4b-12}}{4-b}\right|_{b=3} = 1. \quad (38)$$

In summary, the normalized torque current range of a under condition II is from $2/\sqrt{13}$ to $1/\sqrt{3}$.

In summary, for dual three-phase PMSM drives under single open-phase fault, the optimization variable of proposed online FRML control strategy (k, θ_{shift}) can be expressed as

$$(k, \theta_{\text{shift}}) = \begin{cases} (1/3, 0) & 0 \le a \le 2/\sqrt{13} \\ (\eta(b), 0) & 2/\sqrt{13} \le a \le 1/\sqrt{3} \end{cases}, f \in \{\text{A}, \text{B}, \text{C}\} \quad (39)$$

where the open-circuit fault occurs in the first set of windings. The parameter b can be expressed by $b = 1/a^2$.

It is noteworthy that the analysis above is based on a fault in the first set of three-phase windings, the similar analysis can be also conducted for the fault occurrence in the second set of stator winding. When the open-phase fault occurs in the second set, the setting of k and θ_{shift} of the proposed online FRML control strategy can be updated as

$$(k, \theta_{\text{shift}}) = \begin{cases} (3, 0) & 0 \le a \le 2/\sqrt{13} \\ (r(b), 0) & 2/\sqrt{13} \le a \le 1/\sqrt{3} \end{cases}, f \in \{\text{D}, \text{E}, \text{F}\} \quad (40)$$

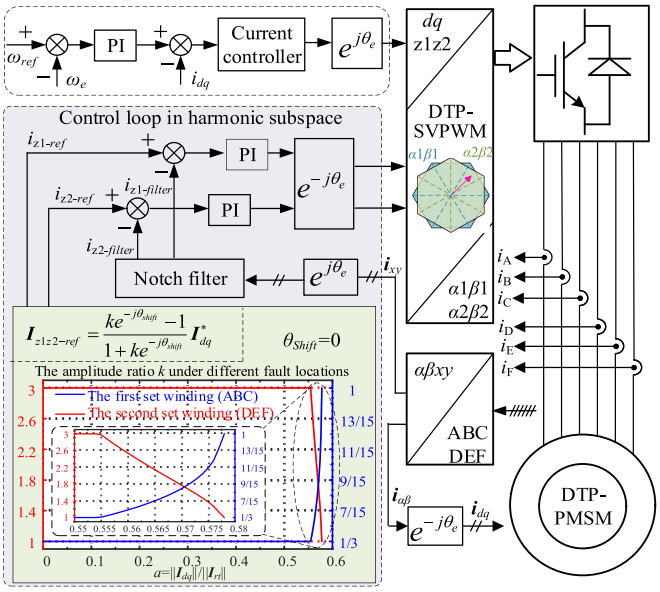

Fig. 6. Implementation of online postfault control strategy for dual three-phase PMSM drive with single phase open-circuit fault.

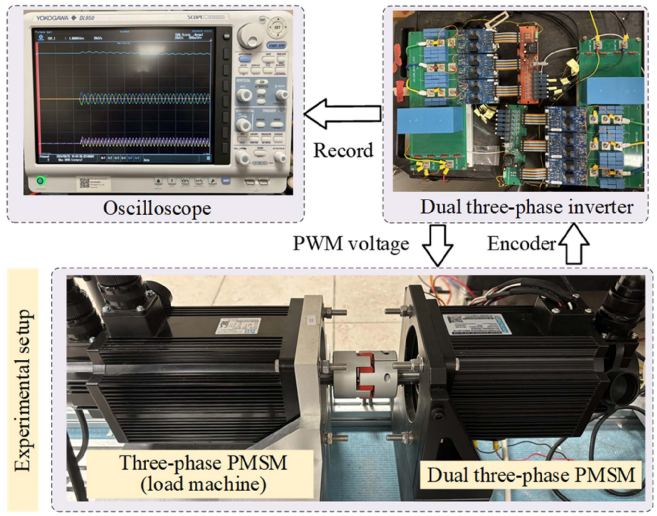

Fig. 7. Experimental setup of dual three-phase PMSM.

where the values of $\eta(b)$ and $r(b)$ are reciprocal of each other: $\eta(b) = 1/r(b)$.

By comparing (39) with (40), it can be observed that the amplitude ratio k of proposed online FRML control strategy becomes reciprocal when the single open-phase fault occurs in different sets of three-phase windings. This reciprocity stems from the inherent structural symmetry of the dual three-phase PMSM.

C. Implementation

According to the aforementioned analytical expression, the proposed online postfault control strategy has been depicted in Fig. 6. Compared to the basic frame of universal control scheme in Fig. 2, the implementation of online postfault control strategy has been highlighted in Fig. 6. The setting of k and θ_{shift} in the proposed online FRML control strategy across the full operating range are illustrated in (39) and (40). At first, the amplitude ratio k is calculated by either (39) or (40) according to whether the fault position is located in the first three-phase set or not. Meanwhile, to mitigate the impact of measurement noise, a low-pass filter can be effectively integrated into the calculation of the current amplitude in the torque subspace. In Fig. 6, the waveform of the amplitude ratio k with respect to the variation of the torque has been illustrated. On the other hand, the phase shift θ_{shift} is always zero for the proposed control method. Once k and θ_{shift} are determined, the $z1$-axis and $z2$-axis current reference of harmonic subspace can be rewritten by (11).

The proposed method requires only simplified fault identification—specifically, determining, which set of three-phase windings is affected—rather than performing detailed fault diagnosis to locate the specific faulty phase. In our implementation, this distinction is made based on a simple current magnitude comparison of positive- and negative-sequence between the two winding sets. If they are identical to each other, the open-phase fault can be located into the specific set of three-phase winding.

TABLE I
PARAMETERS OF DUAL THREE-PHASE PMSM

Parameter	Value	Parameter	Value
Pole pairs	5	Stator resistance (R_s)	0.4 Ω
Rated speed	750 r/min	d-axis inductance (L_D)	1.9 mH
Rated torque	17.8 Nm	q-axis inductance (L_Q)	2.1 mH
Rated current	15 A	Leakage inductance (L_σ)	0.19 mH
Rated power	1.4 kW	PM flux linkage (ψ_m)	0.0795 Wb

IV. Experimental Results

The proposed postfault control strategy is verified by the experiments on a dual three-phase PMSM prototype, the setup of which is shown in Fig. 7. The dual three-phase PMSM is fed by two sets of three-phase inverter sharing with the common dc bus. Meanwhile, the shaft of dual three-phase PMSM is mechanically coupled with another three-phase PMSM, the stator windings of which are connected to the commercial converters. Thus, the three-phase PMSM operates as the load machine and its output torque is controlled by the experimental requirement.

In addition, the field-oriented control control algorithm is implemented in a Texas Instrument TMS320F28377D digital signal processor. For the controller configuration, the control period is 100 μs and the dead-time of PWM signals is 1.0 μs. Table I shows the nominal motor parameters of the dual three-phase PMSM.

A. Comparison of Fault-Tolerant Control Performance

Fig. 8 compares the control performance of three different control methods after the occurrence of single open-phase fault. As shown in Fig. 8(a), there appear some ripples with the peak-to-peak of 1 A in q-axis current when the prefault control method

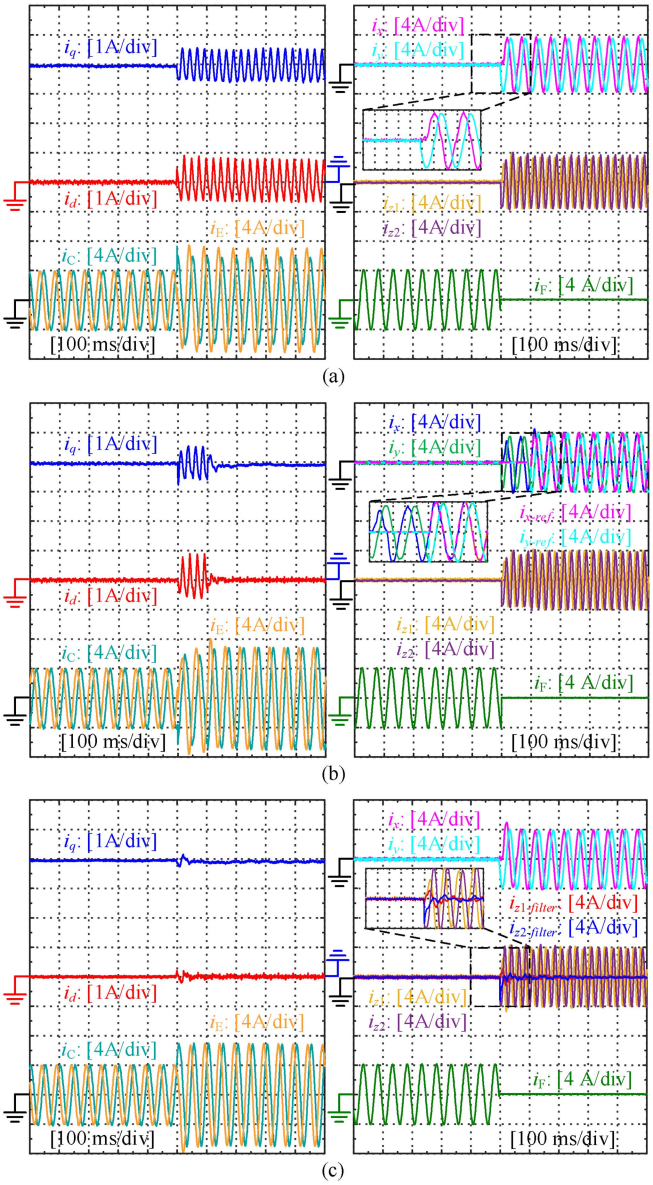

Fig. 8. Performance comparison of different control methods under the open-phase fault of Phase F at 240 r/min @ 4.8 Nm, (a) prefault control method, (b) conventional fault-tolerant method, (c) proposed fault-tolerant method.

designed for healthy condition remains unchanged without the software reconfiguration. After the open-phase fault, the currents of harmonic subspace in stationary *xy* subspace change from zero dc component to ac components with the fundamental frequency, which can be mapped into ac components with double fundamental frequency in synchronous z1z2 subspace.

In order to achieve torque-ripple-free performance, the current references of harmonic subspace in conventional fault-tolerant control methods have been reconfigured as ac value, as shown in Fig. 8(b), and its enlarged view, which is identical to the conclusion in (9). However, the torque ripples inevitably appear in the stage of fault diagnosis, the accurate outcome of which is prerequisite for implementing next conventional fault-tolerant

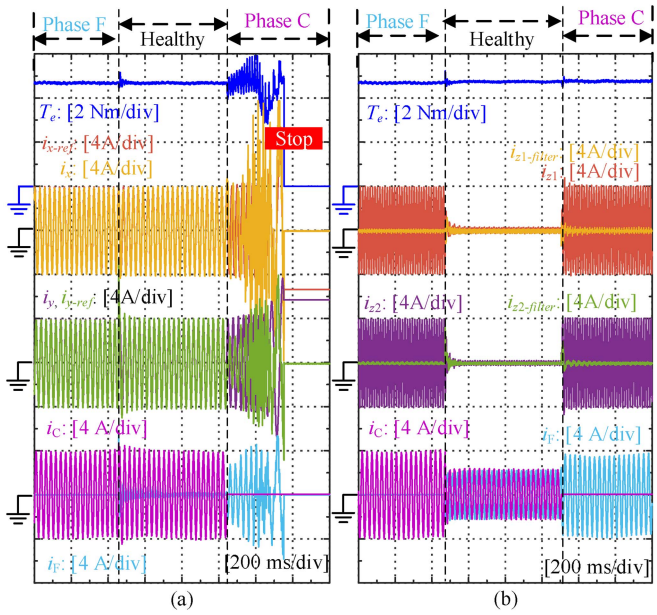

Fig. 9. Fault-tolerant performance of different control methods with the fault location mismatch of open-phase fault at 360 r/min @ 4.8 Nm. (a) Conventional fault-tolerant control method. (b) Proposed fault-tolerant control method.

methods. This is because that the ac current reference must comply the constraints imposed by open circuit fault, as illustrated by (18).

Different from that, the proposed control method employs the notch filter to eliminate the ac components with double fundamental frequency from the current feedback of harmonic subspace after open-phase fault, which can be founded in Fig. 8(c). It can be observed that the proposed control method can achieve seamless transition from healthy condition to fault-tolerant condition without the need of fault diagnosis.

B. Comparison of Robustness With Different Fault Positions

Fig. 9 shows the comparison of fault-tolerant performance of different control methods with the fault location mismatch of open-phase fault. As for the conventional control method, the current reference in software is designed for the open-phase fault of phase F and kept unchanged during the experiments.

As shown in Fig. 9(a), the current of harmonic subspace becomes out of control, and eventually triggers the protection system to shut down when the actual location position of open-circuit fault changes from phase F to phase C. On the contrary, excluding the fluctuation of transient dynamics, there is no ripples in the torque waveforms of Fig. 9(b) with the unchanged software configuration of proposed fault-tolerant control method. Thanks to the separation of the notch filter, the natural fault-tolerant ability without the need of fault diagnosis can be achieved by eliminating interference from fault components at twice the fundamental frequency. Therefore, the proposed fault-tolerant control method has higher robustness over the mismatch of fault location.

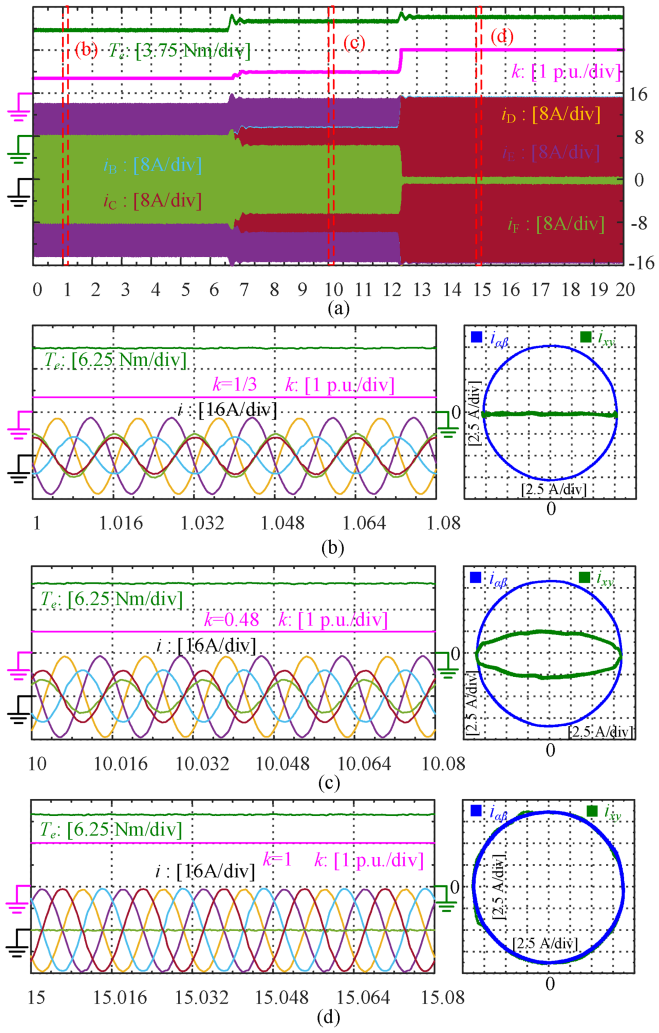

Fig. 10. Phase current and current space vector trajectories of proposed online postfault control strategy with respect to the load increase under the open-phase fault of Phase A at 750 r/min. (a) Whole process. (b) $\|\boldsymbol{I}_{\alpha\beta}\| = 0.523\|\boldsymbol{I}_{rt}\|$. (c) $\|\boldsymbol{I}_{\alpha\beta}\| = 0.566\|\boldsymbol{I}_{rt}\|$. (d) $\|\boldsymbol{I}_{\alpha\beta}\| = 0.577\|\boldsymbol{I}_{rt}\|$.

C. Control Performance Under Full TOR

Fig. 10 presents the phase current and current vector trajectories of online postfault control strategy in the full TOR when the dual three-phase PMSM runs at 750 r/min. The load torque increases from 0.523 p.u. to 0.577 p.u., where the base torque is defined as the rated load with the same phase current limit under healthy conditions. As shown in Fig. 10(a), the amplitude ratio k, the optimization variable of proposed postfault strategy, is changing from 1/3 to 1 during the increase of load torque. The phase shift is always maintained as 0 during the whole process. Meanwhile, the phase current waveforms between healthy phases are also reshaped with the change of the amplitude ratio k under the phase current amplitude limit of 15 A.

Fig. 10(b)–(d) depict the phase currents and current vector trajectories of different load cases $\|\boldsymbol{I}_{\alpha\beta}\| = 0.523\|\boldsymbol{I}_{rt}\|$, $\|\boldsymbol{I}_{\alpha\beta}\| = 0.566\|\boldsymbol{I}_{rt}\|$, and $\|\boldsymbol{I}_{\alpha\beta}\| = 0.577\|\boldsymbol{I}_{rt}\|$, respectively. Among three cases, the same circular trajectories of $\alpha\beta$-axis current in torque subspace illustrate the torque-ripple-free control performance.

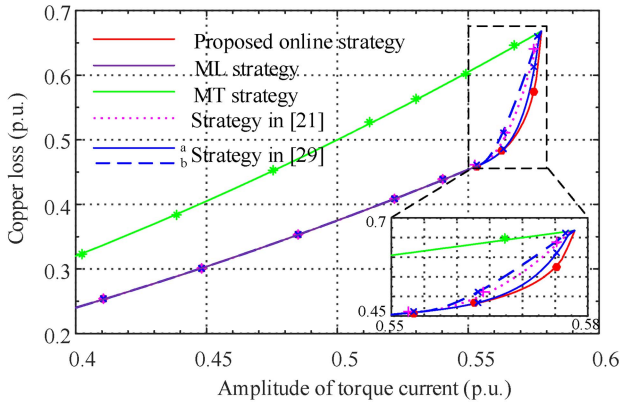

[a] The fault is located in the second set of three-phase winding.
[b] The fault is located in the first set of three-phase winding.

Fig. 11. Comparison of copper loss and operation torque range under different postfault strategies for dual three-phase PMSM under fault-tolerant condition.

In Fig. 10(b), the amplitude ratio of proposed postfault control strategy is calculated as 1/3 according to (39) when $\|\boldsymbol{I}_{\alpha\beta}\| = 0.523\|\boldsymbol{I}_{rt}\|$, and the performance is identical to that of the ML strategy. On the other hand, the amplitude ration of Fig. 10(d) is set as 1 when $\|\boldsymbol{I}_{\alpha\beta}\| = 0.577\|\boldsymbol{I}_{rt}\|$, which indicates that the system status is as same as that of the MT strategy. Fig. 10(c) present the intermediate transition state between the ML strategy and the MT strategy, and its amplitude ratio is 0.48 when $\|\boldsymbol{I}_{\alpha\beta}\| = 0.566\|\boldsymbol{I}_{rt}\|$. In summary, the proposed online postfault control strategy can achieve minimum copper loss during the full torque operation range by optimally transmitting from the ML strategy to the MT strategy as the load torque increases.

In addition, the comparison between different postfault control strategies has been implemented in Fig. 11 in term of the copper loss and the torque operation range. The copper loss and torque current are normalized with respect to their rated values under healthy conditions and are expressed in per unit (p.u.). In the figure, the solid lines represent the theoretical values of the normalized copper loss, while the measured copper losses are marked with symbols such as squares and asterisks. The overlap between the symbols and the lines demonstrates that the experimental results align closely with the theoretical values.

According to the theoretical results of Fig. 11, the operation torque range is 0.555 p.u. for the MT control strategy while it is extended to 0.577 p.u. for the MT control strategy. Compared to the ML and MT strategies, some other control strategies [21], [29] can achieve the same maximum torque operation range as the MT strategy while maintaining the lowest copper losses equivalent to the ML strategy within torque region I (below 0.555 p.u.). When compared with the control method in [21], the proposed method demonstrates up to a 9.0% reduction in copper loss within torque region II (between 0.555 p.u. and 0.577 p.u.). It is also noted that the control performance of online semi-FMRL control strategies [29] varies when the single open-phase fault occurs in the different sets of three-phase winding. Compared with the semi-FMRL strategies [29], the proposed method provides up to a 5.4% or 11.1% relative reduction in copper loss. In summary, relative to the approximate

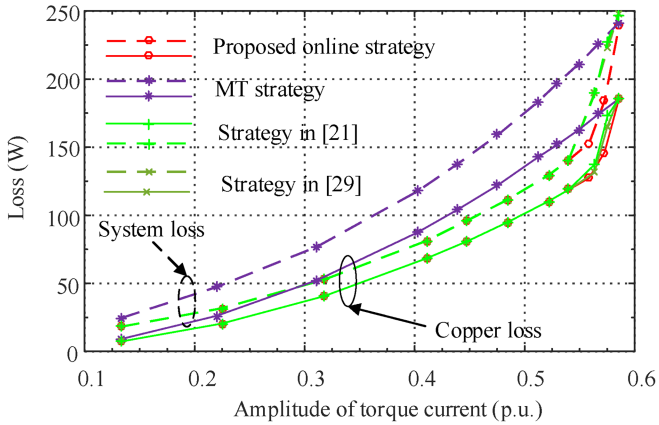

Fig. 12. Experimental results of copper loss and system loss under different postfault strategies for dual three-phase PMSM under fault-tolerant condition.

FRML methods in [21] and [29], the proposed FRML control strategy achieves lower copper losses, particularly within torque region II.

To comprehensively assess the performance of the proposed strategy, both system loss and copper loss were measured at a motor speed of 300 r/min under a single open-phase fault in phase F, as illustrated in Fig. 12. In the figure, the solid line represents the copper loss, while the dotted line indicates the total system loss. In terms of copper loss, the proposed postfault strategy achieves the lowest values across the entire torque range. When inverter losses are also considered, the proposed online FRML strategy results in the minimum total system loss among all postfault control strategies, which is consistent with the findings reported in [30].

D. Discussion

It should be pointed out that the proposed postfault control strategy is limited to asymmetrical six-phase PMSMs (with a 30° phase shift between the two three-phase sets), isolated neutral points, and single open-phase fault conditions, while the space harmonic effects of back-EMF are neglected. It can be inferred that the modeling of the maximum phase current differs significantly across various configurations. Extending the method to accommodate different phase shifts, neutral-point configurations, and additional fault types will be considered in our future work.

In addition, the optimization process can also utilize the currents of the torque subspace for nonsalient dual three-phase PMSMs, given that the d-axis current does not contribute to torque production. However, the resulting reconfigured phase currents are no longer sinusoidal due to the inclusion of current harmonics in the optimization results [15], [16], [17]. Therefore, the proposed postfault control strategies primarily focus on optimizing the currents in the harmonic subspace for the general case.

V. Conclusion

In this article, an online postfault control strategy has been proposed to minimize copper loss in full torque operation range for dual three-phase PMSM under open-circuit fault. Compared to the reconfiguration of current reference of harmonic subspace in conventional control methods, the proposed postfault control strategy employs the online optimizing strategy for the control variables of the amplitude ratio and the phase shift within the frame of the universal control scheme. The proposed postfault control strategy extends the normalized operation torque range to 0.577 p.u., matching that of the MT control strategy. Simultaneously, it achieves the lowest copper losses, equivalent to those of the ML strategy, within torque region I (below 0.555 p.u.). In torque region II (between 0.555 p.u. and 0.577 p.u.), the proposed method maintains the same copper loss as the offline-FRML method, while offering up to a 5.7% or 9.0% relative reduction in copper loss compared to other semi-FRML strategies. Furthermore, the proposed online postfault control strategy reduces the dependency on detailed fault diagnosis. Its implementation requires identifying, which set of three-phase windings the fault is located in, rather than the specific phase in conventional methods, thereby enhancing the robustness against the fault location mismatch. Comprehensive experiments have been given to validate the effectiveness of proposed online postfault control strategy.

Appendix

The feasible region of current coefficient can be expressed for dual three-phase PMSM drive under the open-circuit fault in each phase

$$\text{Phase A}: h_1 = -1; h_2 = 0 \tag{A1}$$

$$\text{Phase B}: h_3 = -\sqrt{3}(h_1+1)/3; h_4 = -\sqrt{3}h_2/3 + 1 \tag{A2}$$

$$\text{Phase C}: h_3 = \sqrt{3}(h_1+1)/3; h_4 = \sqrt{3}h_2/3 + 1 \tag{A3}$$

$$\text{Phase D}: h_3 = \sqrt{3}(h_1-1); h_4 = \sqrt{3}h_2 - 1 \tag{A4}$$

$$\text{Phase E}: h_3 = -\sqrt{3}(h_1-1); h_4 = -\sqrt{3}h_2 - 1 \tag{A5}$$

$$\text{Phase F}: h_3 = 0; h_4 = -1. \tag{A6}$$

References

[1] E. Levi, F. Barrero, and M. J. Duran, "Multiphase machines and drives—Revisited," *IEEE Trans. Ind. Electron.*, vol. 63, no. 1, pp. 429–432, Jan. 2016.

[2] E. Levi, "Advances in converter control and innovative exploitation of additional degrees of freedom for multiphase machines," *IEEE Trans. Ind. Electron.*, vol. 63, no. 1, pp. 433–448, Jan. 2016.

[3] S. Zhu, W. Zhao, G. Liu, Y. Mao, and Y. Sun, "Effect of phase shift angle on radial force and vibration behavior in dual three-phase PMSM," *IEEE Trans. Ind. Electron.*, vol. 68, no. 4, pp. 2988–2998, Apr. 2021.

[4] M. Gu, Z. Wang, and B. Wang, "Optimization of torque ripple for low-carrier-ratio dual three-phase PMSM with pulse pattern control," *IEEE Trans. Power Electron.*, vol. 38, no. 12, pp. 15091–15096, Dec. 2023.

[5] A. G. Yepes, O. Lopez, I. Gonzalez-Prieto, M. Duran, and J. Doval-Gandoy, "A comprehensive survey on fault tolerance in multiphase ac drives part 1: General overview considering multiple fault types," *Machines*, vol. 10, no. 3, 2022, Art. no. 208.
[6] X. Wang, Z. Wang, Z. Xu, J. He, and W. Zhao, "Diagnosis and tolerance of common electrical faults in T-type three-level inverters fed dual three-phase PMSM drives," *IEEE Trans. Power Electron.*, vol. 35, no. 2, pp. 1753–1769, Feb. 2020.
[7] A. G. Yepes, I. Gonzalez-Prieto, O. Lopez, M. Duran, and J. Doval-Gandoy, "A comprehensive survey on fault tolerance in multiphase ac drives part 2: Phase and switch open-circuit faults," *Machines*, vol. 10, no. 3, 2022, Art. no. 221.
[8] Y. Zhao and T. A. Lipo, "Space vector PWM control of dual three-phase induction machine using vector space decomposition," *IEEE Trans. Ind. Appl.*, vol. 31, no. 5, pp. 1100–1109, Sep./Oct. 1995.
[9] Y. Hu, Z. Q. Zhu, and M. Odavic, "Comparison of two-individual current control and vector space decomposition control for dual three-phase PMSM," *IEEE Trans. Ind. Appl.*, vol. 53, no. 5, pp. 4483–4492, Sep./Oct. 2017.
[10] W. N. W. A. Munim, M. J. Duran, H. S. Che, M. Bermúdez, I. González-Prieto, and N. A. Rahim, "A unified analysis of the fault tolerance capability in six-phase induction motor drives," *IEEE Trans. Ind. Electron.*, vol. 32, no. 10, pp. 7824–7836, Oct. 2017.
[11] H. S. Che, M. J. Duran, E. Levi, M. Jones, W.-P. Hew, and N. A. Rahim, "Post-fault operation of an asymmetrical six-phase induction machine with single and two isolated neutral points," *IEEE Trans. Power Electron.*, vol. 29, no. 10, pp. 5406–5416, Oct. 2014.
[12] S. Dwari and L. Parsa, "An optimal control technique for multiphase PM machines under open-circuit faults," *IEEE Trans. Ind. Electron.*, vol. 55, no. 5, pp. 1988–1995, May 2008.
[13] J.-R. Fu and T. A. Lipo, "Disturbance-free operation of a multiphase current-regulated motor drive with an opened phase," *IEEE Trans. Ind. Appl.*, vol. 30, no. 5, pp. 1267–1274, Sep./Oct. 1994.
[14] F. Baneira, J. Doval-Gandoy, A. G. Yepes, Ó. López, and D. Pérez-Estévez, "Control strategy for multiphase drives with minimum losses in the full torque operation range under single open-phase fault," *IEEE Trans. Power Electron.*, vol. 32, no. 8, pp. 6275–6285, Aug. 2017.
[15] X. Wang, Z. Wang, M. He, Q. Zhou, X. Liu, and X. Meng, "Fault tolerant control of dual three-phase PMSM drives with minimized copper loss," *IEEE Trans. Power Electron.*, vol. 36, no. 11, pp. 12938–12953, Nov. 2021.
[16] G. Feng, C. Lai, W. Li, J. Tjong, and N. C. Kar, "Open-phase fault modeling and optimized fault-tolerant control of dual three-phase permanent magnet synchronous machines," *IEEE Trans. Power Electron.*, vol. 34, no. 11, pp. 11116–11127, Nov. 2019.
[17] L. Jin, Y. Mao, X. Wang, P. Shi, L. Lu, and Z. Wang, "Optimization-based maximum-torque fault-tolerant control of dual three-phase PMSM drives under open-phase fault," *IEEE Trans. Power Electron.*, vol. 38, no. 3, pp. 3653–3663, Mar. 2023.
[18] A. G. Yepes, A. Shawier, W. E. Abdel-Azim, A. S. Abdel-Khalik, S. Ahmed, and J. Doval-Gandoy, "General online current-harmonic generation for increased torque capability with minimum stator copper loss in fault-tolerant multiphase induction motor drives," *IEEE Trans. Transp. Electrific.*, vol. 9, no. 3, pp. 4650–4667, Sep. 2023.
[19] H. Zheng, X. Pei, C. Liagas, C. Brace, and X. Zeng, "Extended minimum copper loss range fault-tolerant control for dual three-phase PMSM," *IEEE Trans. Ind. Appl.*, vol. 60, no. 4, pp. 6263–6276, Jul./Aug. 2024.
[20] J. Sun, Z. Liu, Z. Zheng, and Y. Li, "An online global fault-tolerant control strategy for symmetrical multiphase machines with minimum losses in full torque production range," *IEEE Trans. Power Electron.*, vol. 35, no. 3, pp. 2819–2830, Mar. 2020.
[21] G. Yang, H. Hussain, S. Li, J. Zhang, and J. Yang, "A unified fault-tolerant strategy for multiphase machine with minimum losses in full torque operation range based on closed-form expressions," *IEEE Trans. Power Electron.*, vol. 37, no. 10, pp. 12463–12473, Oct. 2022.
[22] Q. Geng, Z. Li, H. Wang, G. Zhang, and Z. Zhou, "Natural fault-tolerant control with minimum copper loss in full torque operation range for dual three-phase PMSM under open-circuit fault," *IEEE Trans. Power Electron.*, vol. 39, no. 1, pp. 1279–1291, Jan. 2024.
[23] I. G. Prieto, M. J. Duran, P. Garcia-Entrambasaguas, and M. Bermudez, "Field-oriented control of multiphase drives with passive fault tolerance," *IEEE Trans. Ind. Electron.*, vol. 67, no. 9, pp. 7228–7238, Sep. 2020.
[24] Z. Song, Y. Jia, and C. Liu, "Open-phase fault-tolerant control strategy for dual three-phase permanent magnet synchronous machines without controller reconfiguration and fault detection," *IEEE Trans Power Electron.*, vol. 38, no. 1, pp. 789–802, Jan. 2023.
[25] Q. Liu, L. Xiao, Q. Wu, X. Zhao, and Y. Liu, "An adaptive fault-tolerant control without fault location of open-phase fault for dual three-phase PMSM drive system," *IEEE J. Emerg. Sel. Topics Power Electron.*, Jun. 2025, vol. 13, no. 3, pp. 3516–3528..
[26] P. Shi, X. Wang, X. Meng, M. He, Y. Mao, and Z. Wang, "Adaptive fault-tolerant control for open-circuit faults in dual three-phase PMSM drives," *IEEE Trans. Power Electron.*, vol. 38, no. 3, pp. 3676–3688, Mar. 2023.
[27] K. Yu, Z. Wang, M. Gu, and X. Wang, "Universal control scheme of dual three-phase PMSM drives with single open-phase fault," *IEEE Trans. Power Electron.*, vol. 37, no. 12, pp. 14034–14039, Dec. 2022.
[28] K. Yu, Z. Wang, X. Wang, M. Gu, J. Hang, and S. Ding, "Post-fault strategy of universal control for dual three-phase PMSM under single open-phase fault considering current amplitude," *IEEE Trans. Transp. Electrific.*, vol. 10, no. 3, pp. 7456–7466, Sep. 2024.
[29] K. Yu and Z. Wang, "An online fault-tolerant optimization strategy of copper loss for dual three-phase PMSM drives," in *Proc. ITEC Asia-Pacific*, Haining, China, 2022, pp. 1–5.
[30] F. Baneira, J. Doval-Gandoy, A. G. Yepes, Ó. López, and D. Pérez-Estévez, "Comparison of postfault strategies for current reference generation for dual three-phase machines in terms of converter losses," *IEEE Trans. Power Electron.*, vol. 32, no. 11, pp. 8243–8246, Nov. 2017.

Kailiang Yu (Member, IEEE) received the B.E. degree from Southeast University, Nanjing, China, in 2016, the M.S. degree from Huazhong University of Science and Technology, Wuhan, China, in 2019, and the Ph.D. degree from Southeast University, Nanjing, China, in 2023, all in electrical engineering.

He is currently a Postdoctoral Research Fellow with Nanyang Technological University, Singapore. His research interests include the control of multiphase permanent magnet synchronous motor, such as parameter estimation, position sensorless control, and fault-tolerance control.

Zheng Wang (Senior Member, IEEE) received the B.Eng. and M.Eng. degrees in Electrical Engineering from Southeast University, Nanjing, China, in 2000 and 2003, respectively, and the Ph.D. degree in Electrical Engineering from The University of Hong Kong, Hong Kong, in 2008.

From 2008 to 2009, he was a Postdoctoral Fellow with Ryerson University, Toronto, ON, Canada. He is currently a Full Professor with the School of Electrical Engineering, Southeast University, China. His research interests include electric drives, power electronics, and renewable power generation.

Dr. Wang received IEEE PES Chapter Outstanding Engineer Award and Outstanding Young Scholar Award of Jiangsu Natural Science Foundation of China. He is serving as the Asia Liaison of Transportation System Committee for IEEE IAS, the Vice Chairman of Technical Committee of Renewable Energy System for IEEE IES, and an Associate Editor for IEEE TRANSACTIONS ON INDUSTRY APPLICATIONS. He is an IET Fellow and an IEEE VTS Distinguished Lecturer.

Huanzhi Wang (Graduate Student Member, IEEE) received the B.Eng. degree in electrical engineering and automation from Dalian Maritime University, Dalian, China, in 2020, and the M.Sc. degree in power engineering in 2021 from Nanyang Technological University, Singapore, where he is currently working toward the Ph.D. degree in Electrical Engineering with the School of Electrical and Electronic Engineering.

His research interests include power electronics, electric motor drives, and advanced control strategies.

Chenhao Zhao (Graduate Student Member, IEEE) received the B.Eng. degree in electrical and electronic engineering (with first class hons.) from the University of Nottingham, Ningbo, China, in 2020, and the M.Sc. degree in power engineering in 2021 from Nanyang Technological University, Singapore, where he is currently working toward the Ph.D. degree with the School of Electrical and Electronic Engineering.

His research interests include electric machine drives, nonlinear control, and intelligent control.

Xuhui Zhu (Member, IEEE) received the B.Sc. and Ph.D. degrees in electrical engineering from Jiangsu University, Zhenjiang, China, in 2015 and 2021, respectively.

From 2022 to 2024, he was a Postdoctoral Research Fellow with the School Electrical and Electronic Engineering, Nanyang Technological University, Singapore. He is currently a Lecturer with Nantong University, Nantong, China. His research interests include electrical motor design, electromagnetic field analysis, and motor control.

Christopher H. T. Lee (Senior Member, IEEE) received the B.Eng. (first class hons.) and the Ph.D. degrees in electrical engineering from the Department of Electrical and Electronic Engineering, The University of Hong Kong, Hong Kong, in 2009 and 2016, respectively.

He is currently an Associate Professor with Nanyang Technological University, Singapore. He was a Postdoctoral Fellow and then a Visiting Assistant Professor at Massachusetts Institute of Technology, USA. He is an Associate Editor for IEEE TRANSACTIONS ON INDUSTRIAL ELECTRONICS, IEEE TRANSACTIONS ON ENERGY CONVERSION, and *IET Renewable Power Generation*. He is currently the Chair of Motor Subcommittee of IEEE PES Electric Machinery Committee. He was the Chair of IEEE Vehicular Technology Society Singapore Section Chapter in 2023–2025. He is a Chartered Engineer in Hong Kong. He has authored and coauthored 2 books, 4 books chapters, and more than 270 referred papers in the area of his research interests, which include electric machines and drives, renewable energies, and electromechanical propulsion technologies.

Dr. Lee is a Fellow of the Institution of Engineering and Technology, U.K. He was a recipient of the 10th Nagamori Award in 2024, IAS Myron Zucker Student-Faculty Grant in 2023, JSPS Fellowship in 2023, MDPI Energies Young Investigator Award in 2022, NRF Fellowship in 2020, Nanyang Assistant Professorship in 2019, Li Ka Shing Prize (the best Ph.D. thesis prize) in 2017 and Croucher Foundation Fellowship in 2016, and 8 best paper awards, including Best Paper Awards in IEEE Transactions on Energy Conversion in 2022 and 2024.